NOTES AND CORRESPONDENCE

Statistical Analysis and Wavenumber-Frequency Spectra of the 500 mb Geopotential along 50°S

K. FRAEDRICH AND E. KIETZIG

Institut für Meteorologie, Freie Universität Berlin, D-1000 Berlin 33, W-Germany

ABSTRACT

Daily 500 mb geopotentials gridded along 50°S are statistically analyzed for five summer and winter seasons (1959–64): 1) to establish climatic statistics of the macro-turbulent processes in the Southern Hemisphere westwind zone, and 2) to obtain a zonally averaged spectral description of the space–time (wavenumber–frequency) structure of midlatitude disturbances of the Southern Hemisphere. In contrast to the Northern Hemisphere, two (instead of three) separated variance maxima are observed in the wavenumber–frequency spectra of the meridional component which contribute to transient eddy variance. They occur in the long ($k = 4$–5, $p = 6$–12 days, $c \approx 6$ m s^{-1}) and short ($k = 6$–7, $p < 6$ days, $c \approx 11$ m s^{-1}) period range of eastward traveling waves.

1. Introduction

Some interesting features appear in zonal-time statistics and spectral analyses of the 500 mb geopotential in the midlatitudes of the summer and winter Northern Hemisphere (NH): 1) Three significantly separated variance maxima are observed in the wavenumber–frequency spectra contributing to the transient eddy variance: ultralong waves (wavenumber k = 1–4) are quasi-stationary oscillations with periods $p > 12$ days, long waves ($k = 5$–6) and short waves ($k = 7$–9) are propagating eastward with periods p = 5–12 and $p < 5$ days, respectively. In summer these peaks are less intense and shifted to higher wavenumbers (Hayashi and Golder, 1977; Fraedrich and Böttger, 1978). 2) For both seasons the total zonal-time variance remains approximately the same; thus, standing eddy variance seems to be compensated by transient cell and transient eddy variance. Local time statistics, in particular higher moments, allow some additional insight into the zonal inhomogeneities averaged out by zonal-time statistics (White, 1980).

In this note we supplement these results by a study of the 500 mb geopotential in the Southern Hemisphere (SH) midlatitudes along 50°S to obtain similar statistical information, to provide an empirical background for the analysis of output data of model experiments (e.g., Hayashi and Golder, 1977), and to add details to the SH eddy statistics. This includes the evaluation of disturbances in the wavenumber-frequency domain (in a zonally averaged sense), the zonal variability of local frequency distributions and their moments, and the use of another data set.

First, the data set and the method of analysis are introduced in Section 2; Section 3 presents the zonal-time statistics; in Section 4 the transient eddy variance is decomposed in the wavenumber–frequency domain to determine the dominating scales of time fluctuating processes in the Southern Hemisphere (SH) circulation. Then, in Section 5 some regional characteristics are described by the analysis of local statistics.

2. Data and method of analysis

Daily Southern Hemispheric 500 mb charts published by the South African Weather Service (Notos, 1964–70) are based on all types of available data which can possibly be used for an *a posteriori* daily synoptic analysis. The procedure of map construction and extrapolation has been described by Taljaard and van Loon (1960, 1964). As the main storm track in the SH is along 50°S, it appears reasonable to choose this latitude circle for a statistical study of disturbances in the SH midlatitudes. Thus, daily geopotential heights $Z(\lambda, t)$ of the last five summer and winter seasons (1959–64) published by the South African Weather Service are digitized on a 10° longitude grid (λ) around 50°S. The scale of the smallest eddy resolved will be 1500 km. The data sets have an equal length of 120 days beginning on 1 November and on 1 May.

When averaged with respect to longitude and time, the variable $Z(\lambda, t)$ is given by four terms:

$$Z(\lambda, t) = [Z]_{\lambda,t} + ([Z]_\lambda)_t + ([Z]_t)_\lambda + (Z)_{\lambda,t},$$

where the time t and zonal λ averages and departures are denoted by [ ]$_t$, [ ]$_\lambda$ and ( )$_t$, ( )$_\lambda$, respectively. The first term on the right hand side is the

zonal-time average attributed to the time-mean meridional circulation; the second term represents the fluctuations in time of the zonal mean (transient cell); the third the longitudinal fluctuations of the time averages (stationary eddies); and, finally, the fourth term represents the combined zonal-time fluctuations (transient eddies). Only the last three terms contribute to the total zonal-time variance $\text{Var}Z(\lambda, t)$, because

$$[Z^2]_{\lambda,t} = [Z]_{\lambda,t}^2 + \text{Var}Z$$

$$\text{Var}Z(\lambda, t) = [([Z]_\lambda)_t^2]_{\lambda,t} + [([Z]_t)_\lambda^2]_{\lambda,t} + [(Z)_{\lambda,t}^2]_{\lambda,t}.$$

For each seasonal data set (36 grid points × 120 days) all terms contributing to the total variance are deduced. By applying zonal Fourier and time spectral analyses, the transient eddy variance is decomposed in the wavenumber–frequency domain following the procedure described by Hayashi (1971, 1973):

$$[(Z)_{\lambda,t}^2]_{\lambda,t} = \sum_{k=0}^{\infty} \sum_{f=0}^{\infty} \{E_z(k, +f) + E_z(k, -f)\}.$$

Here $E_z(k, \pm f)$ is the two-sided variance density spectrum of the geopotential Z in a wavenumber (k)–frequency (f) domain. It is obtained by first expanding $(Z)_{\lambda,t}$ into zonal Fourier harmonics and then computing power-, co- and quadrature spectra of the cosine (C_k) and sine (S_k) components. The propagating variance density spectrum $PR(k, f)$ is defined by the difference of the eastward and westward contribution of E_z and equals the quadrature spectrum Q_f. It gives

the lower limit of traveling wave variance, while the eastward or westward spectra give the upper limit:

$$PR(k, f) = |Q_f(C_k, S_k)|.$$

The propagation direction can be inferred from the sign of Q_f and means which of the eastward and westward moving component is dominant. If both components are coherent, time fluctuations fixed in longitude (standing fluctuations) result from waves of the same wavenumber and frequency-band traveling in opposite directions (Hayashi, 1977). The Fourier harmonics are cut off at wavenumber $k = 12$, beyond which the remaining variance appears to be negligibly small ($<5\%$). The spectra are computed by using a lag-correlation method up to a 20-day lag. Smoothing is accomplished by applying the Tukey window with an equivalent band width of $b = 0.0665$ cpd and approximately 15 degrees of freedom for each of the 41 spectral estimates.

3. Zonal-time statistics

Some details of the zonal-time statistics at 50°S for individual years and SH and NH averages are briefly summarized (Table 1). General agreement with previous studies (Trenberth, 1981a,b) is found in the following two points: 1) The total zonal-time variances change relatively little from summer to winter; additionally, individual winters (summers) deviate less than 10% (15%) about their average. This is a

TABLE 1. Zonal-time variance of the geopotential at 500 mb and 50°S for five summer and winter seasons, and their averages: variances of transient cell (time fluctuations of the zonal means), stationary eddies (longitudinal fluctuations of the time averages), and transient eddies ($\sum_{k=1}^{12} \sum_{f=0}^{20} \{E(k, f) + E(k, -f)\}$; zonal-time fluctuations, respectively). Total variance of zonal-time fluctuations is the sum of these terms. Propagating variance is part of the transient eddy variance, percentage given in brackets. Geopotential units are in gpdm, units of variance terms are in gpdm². NH averages are added for comparison.

|	Zonal-time mean of geopotential	Variance of transient cell	Variance of stationary eddies	Variance of transient eddies	Propagating variance	Total variance of zonal-time fluctuations
Summer						
59/60	543.8	16.6	64.7	108.1	49.1 (45%)	189.4
60/61	541.6	13.3	61.3	114.2	51.3 (45%)	188.8
61/62	545.3	18.8	50.4	100.4	44.9 (45%)	169.6
62/63	543.4	30.0	78.2	113.1	49.4 (44%)	221.3
63/64	541.4	20.6	37.8	122.3	50.0 (41%)	180.7
SH average (50°S)	543.1	19.9	58.5	111.6	48.9 (44%)	190.0
NH average (50°N)	564.5	44.7	16.3	73.3	26.9 (37%)	134.3
Winter						
1960	535.2	20.3	65.2	131.2	70.0 (53%)	216.7
1961	534.4	22.1	36.1	146.0	71.9 (49%)	204.2
1962	534.8	18.4	67.2	123.8	62.4 (50%)	209.4
1963	533.5	21.7	26.8	141.7	66.3 (47%)	190.2
1964	532.7	17.0	33.1	131.1	60.4 (46%)	181.2
SH average (50°S)	534.1	19.9	45.7	134.8	66.2 (49%)	200.4
NH average (50°N)	537.1	33.4	117.9	157.2	58.8 (37%)	308.5
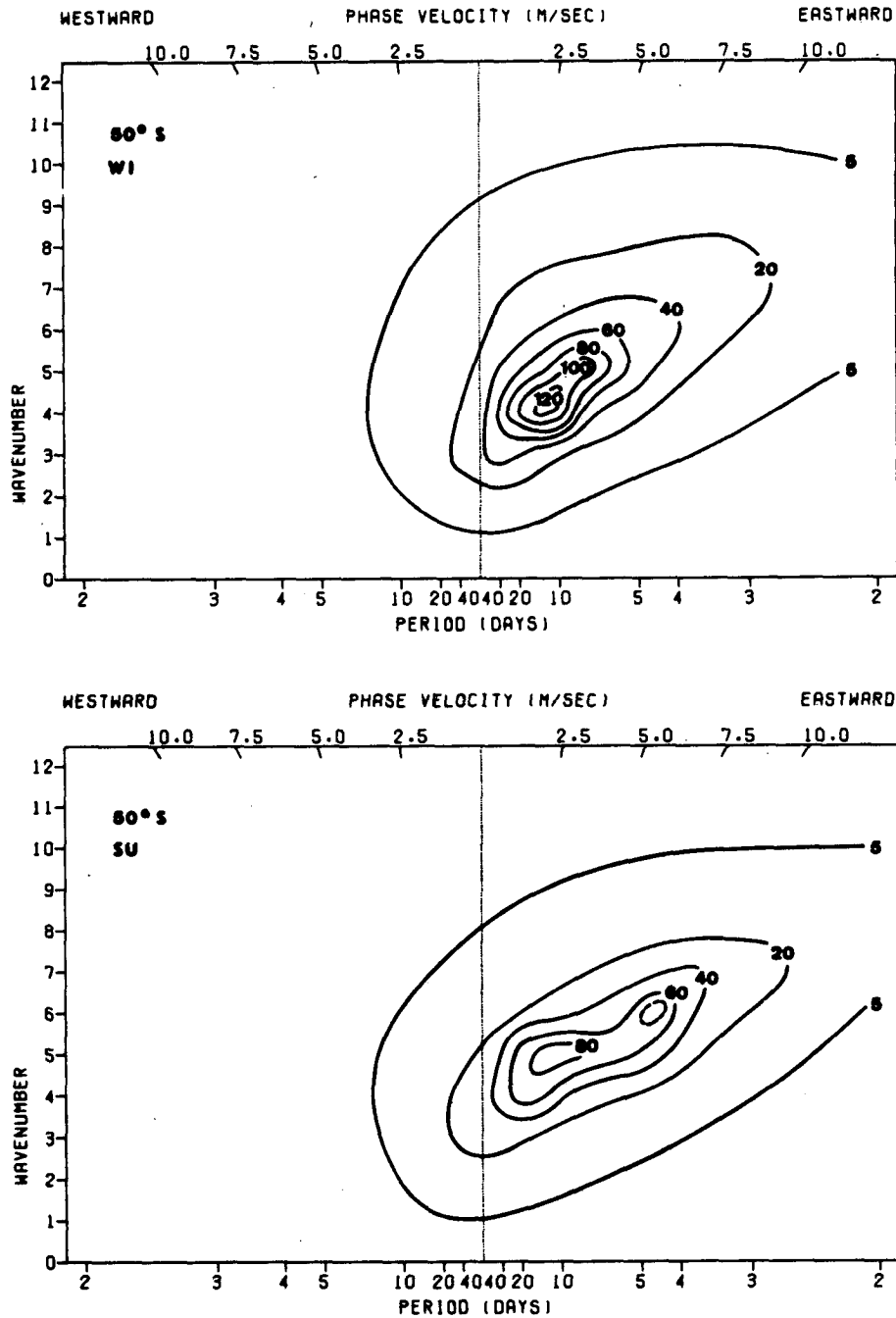
FIG. 1. Wavenumber–frequency contours of power spectrum density (m^2 $s^{-2}/\Delta f$) of the meridional geostrophic wind V_g at 500 mb along 50°S. Average for Winter (WI) and Summer (SU). The spectral estimates contributing to transient eddy variance are computed for discrete wavenumbers k and frequencies f, then interpolated linearly and, in addition, smoothed manually, leaving the main features of the spectra unchanged. The linear frequency axis is labeled in period p of days, the upper abscissa gives the related phase velocity $c = Lp^{-1}$ in m s^{-1}, where L is the wavelength at 50°S. The isolines of c converge at wavenumber $k = 0$ and period $p = \infty$.

known feature of the SH and different from the NH circulation. In the SH the zonal-time variance is in winter (summer) 35% smaller (larger) than in the NH.

2) The stationary eddies account for the time-mean zonal asymmetries. They are more intense in summer and show less intensity in winter than in the NH.
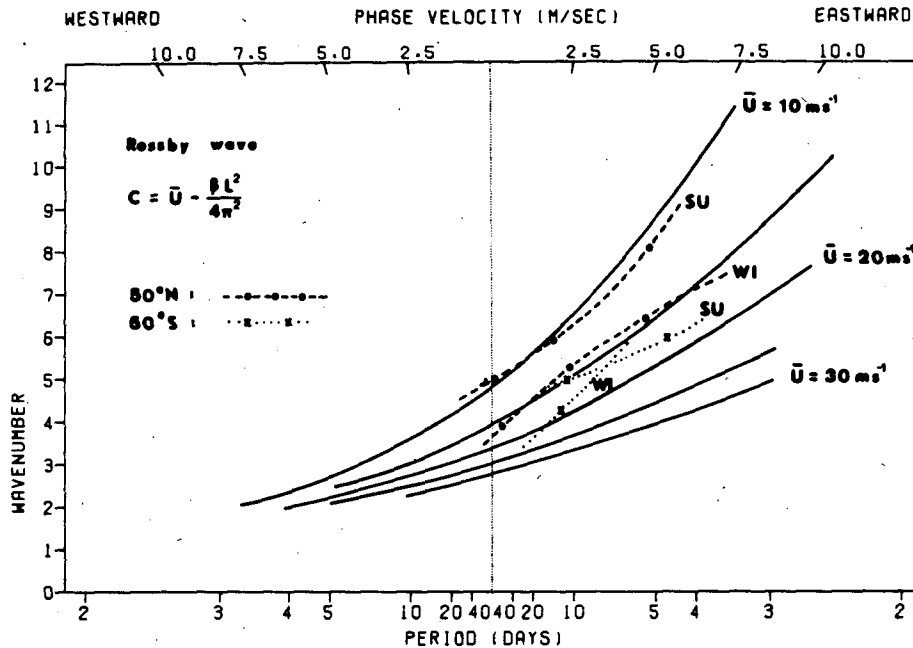
FIG. 1. (*Continued*) Phase velocity c_R (full lines) of Rossby waves at 50° latitude for different values of the zonal flow $\bar{U}$. "Dispersion lines" of SH summer and winter spectra (dotted) are compared with NH spectra (dashed).

Along 50°S stationary eddies attain approximately half (three times) the magnitude of their winter (summer) counter parts along 50°N.

Some additional results should be noted: 3) The transient cell variance is smaller in the SH than in the NH and hardly changes from summer to winter. 4) The transient eddy variance is, in contrast to the stationary eddy variance, larger in winter than in summer seasons. A considerable amount, 44–49%, is expended by propagating waves. NH propagating eddies are less efficient; i.e. they consume only 37% of the transient eddy variance. The remaining part of transient eddy variance at the "zero" frequency may be due to quasi-standing fluctuations (temporally varying and spatially fixed) and to seasonal trend or cycle. In addition, the geopotential spectra (Fig. 2) show maxima of variance at large periods for the quasi-stationary waves 1 and 2. These waves are not purely standing but have propagating components, eastward and westward in summer and mainly eastward in winter. 5) Comparing the seasonal averages of summer and winter, the stationary and transient eddies seem to compensate one another; when stationary eddy variance is large, transient eddy variance tends to be reduced (summer) and *vice versa* (winter). Enhancement of transient eddy variance in winter seems to be accomplished by eastward traveling long and short waves, and not by the remaining quasi-standing time fluctuations. This is indicated by the seasonal variation of the propagating variance (Table 1). A similar compensation may be observed in the

Northern Hemisphere but involving the ultra-long wave regime of individual winters (Böttger and Fraedrich, 1980).

4. Wavenumber–frequency spectra

The transient eddy variance of the geostrophic meridional wind $[(V_g)^2_{\lambda,t}]_{\lambda,t}$ is spectrally decomposed in the wavenumber–frequency domain to derive the dominant space and time scales of SH midlatitude motion systems. The variance is proportional to kinetic energy of the meridional geostrophic wind component of the transient eddies. Two-sided variance density spectra are computed at a wavenumber k to define the components of eastward $(+f)$ and westward $(-f)$ propagating waves for a frequency band centered at f:

$$E_z(k, \pm f) = \tfrac{1}{4}\{P_f(C_k) + P_f(S_k)\} \pm \tfrac{1}{2}Q_f(C_k, S_k),$$

where P_f and Q_f are the power- and quadrature spectral densities of the longitude and time dependent transient meridional geostrophic wind $(V_g)_{t,\lambda}$ expanded into Fourier harmonics: $C_k(t) \cos k\lambda + S_k(t) \times \sin k\lambda$.

Two wavenumber–frequency diagrams (Fig. 1) show the average conditions for the five summer and winter seasons. The spectral density maxima are arranged in a band orientated from smaller wavenumbers and long periods to large wavenumbers and short periods. A "dispersion line" connecting these peaks describes the phase velocity c changing with wave-
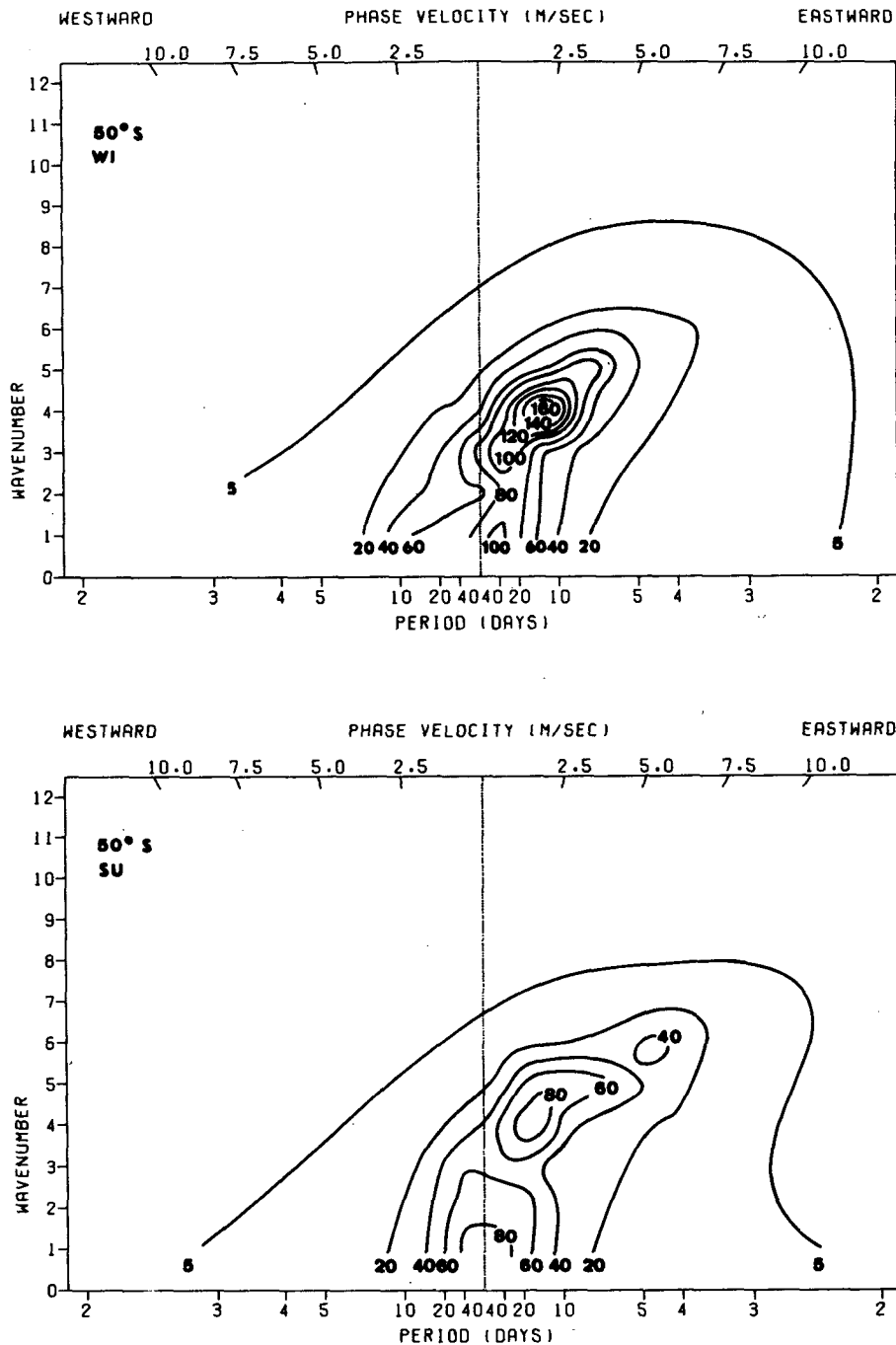
FIG. 2. As in Fig. 1, but for geopotential.

number k. On this line two peaks appear in the spectra which suggest a division of the SH atmospheric motion scales into two main regimes. Variance minima in the wavenumber–frequency domain define the scale-related wavenumber and period intervals. In the SH summer the two spectral maxima can be defined by

1) "long" period disturbances, which are caused by waves (period p = 6–12 days, k = 4–5) traveling eastward with a phase velocity $c \approx 6$ m s^{-1}.

2) "short" period disturbances, which are associated with waves (period p < 6 days and wavenumber k = 6–7) progressing eastward with a phase velocity $c \approx 11$ m s^{-1}.

The spectra of the 500 mb geopotential transient eddy variance $[(Z)^2_{\lambda,t}]_{\lambda,t}$ are presented in Fig. 2. Compared with the geostrophic wind the variance maximum is shifted to wavenumber 4 where it is more intense in winter than in summer. Thus, the large variance of the geostrophic meridional wind component at wavenumber 5 seems to be caused by an evident geostrophical suppression of the longer waves. The spectral peak of short period fluctuations in summer remains well defined in both the geopotential and the geostrophic wind v_g.

In SH winters the "dispersion line" (Fig. 1) is shifted towards smaller wavenumbers and the disturbances show a considerably enhanced intensity. The long waves clearly exhibit maximum intensity for both wavenumber $k = 5$ and 4 at periods $p \approx 6$ to 10 days. The separate peak of shorter period fluctuations, which is well defined in summer, is smoothed out in winter by the seasonal averaging, because in our data set, short period disturbances along 50°S show a large winter-to-winter variability. A Hovmöller diagram analysis of migrating 500 mb troughs (Fig. 3, see also van Loon, 1965) is in good agreement with the results of the cross-spectral analysis.

In the NH midlatitudes the wavenumber–frequency spectra along 50°N show three distinct peaks. The most intense spectral peak of the ultralong periods ($k = 1$–3, $p \approx 20$ days), generated by progressive and retrogressive waves of different vertical structure, does not appear as a well defined regime in the SH midlatitudes. Accordingly, in comparison with 50°N purely westward propagating waves along 50°S contribute only a small amount of variance to the meridional components of the transient eddies.

Thus, in the SH large contributions to the total transient variance come from waves traveling eastward along 50°S. In a barotropic, non-divergent atmosphere with infinite lateral boundaries, Rossby waves of the same phase speed would propagate in zonal current of 15–20 m s^{-1} (Fig. 1, bottom), which approximately corresponds to the observed longitudinally averaged 500 mb geostrophic zonal wind component along 50°S (see Trenberth, 1981a,b). Rossby phase velocity, however, can only be a lower limit as divergence effects and lateral boundaries tend to increase the speed of propagation.

5. Zonal inhomogeneities: mean, variance, skewness, kurtosis

In the preceeding two sections, the statistics of SH disturbances along 50°S have been described in terms of zonal averages and without explicitly resolving longitudinal variations. Thus, some regional characteristics (as they appear in this data set) are discussed. At each gridpoint along 50°S seasonal distributions of daily 500 mb geopotential heights $Z(t, \lambda)$ and related statistical information are determined from the

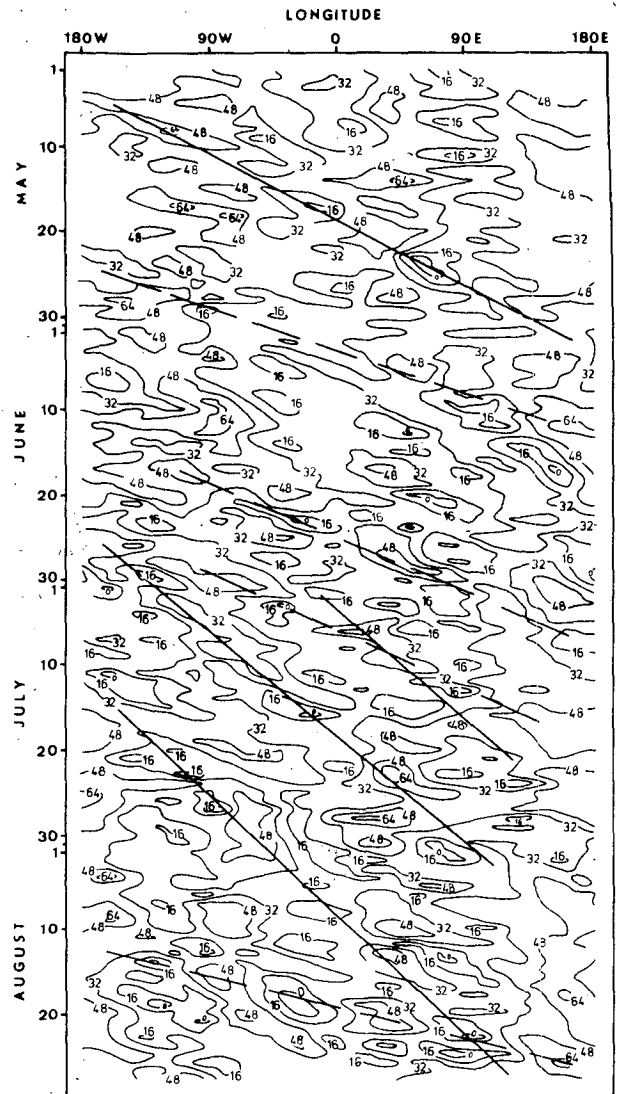FIG. 3. Time–longitude (Hovmöller) diagram of 500 mb geopotential (gpdm) for the Southern Hemisphere winter 1961 at 50°S. Full (dashed) lines indicate long (short) traveling troughs.

(5 × 120) available observations. This statistic includes extrema, modes and moments m_n:

$$m_n(\lambda) = [(Z(\lambda, t) - [Z(\lambda, t)]_t)^n]_t$$

as deviations from the mean $[Z(\lambda, t)]_t$.

The mean and the variance of an empirical distribution determine the theoretical Gaussian fit to that distribution. Deviations from such a Gaussian reference profile become evident if the observed skewness $(m_3 m_2^{-3/2})$ and kurtosis $(m_4 m_2^{-2} - 3)$ do not vanish (as they do for Gaussian processes). Thus, these normalized higher moments provide some useful quantitative information on the structure of the observed distribution and, possibly, the underlying processes. Results are statistically meaningful if the
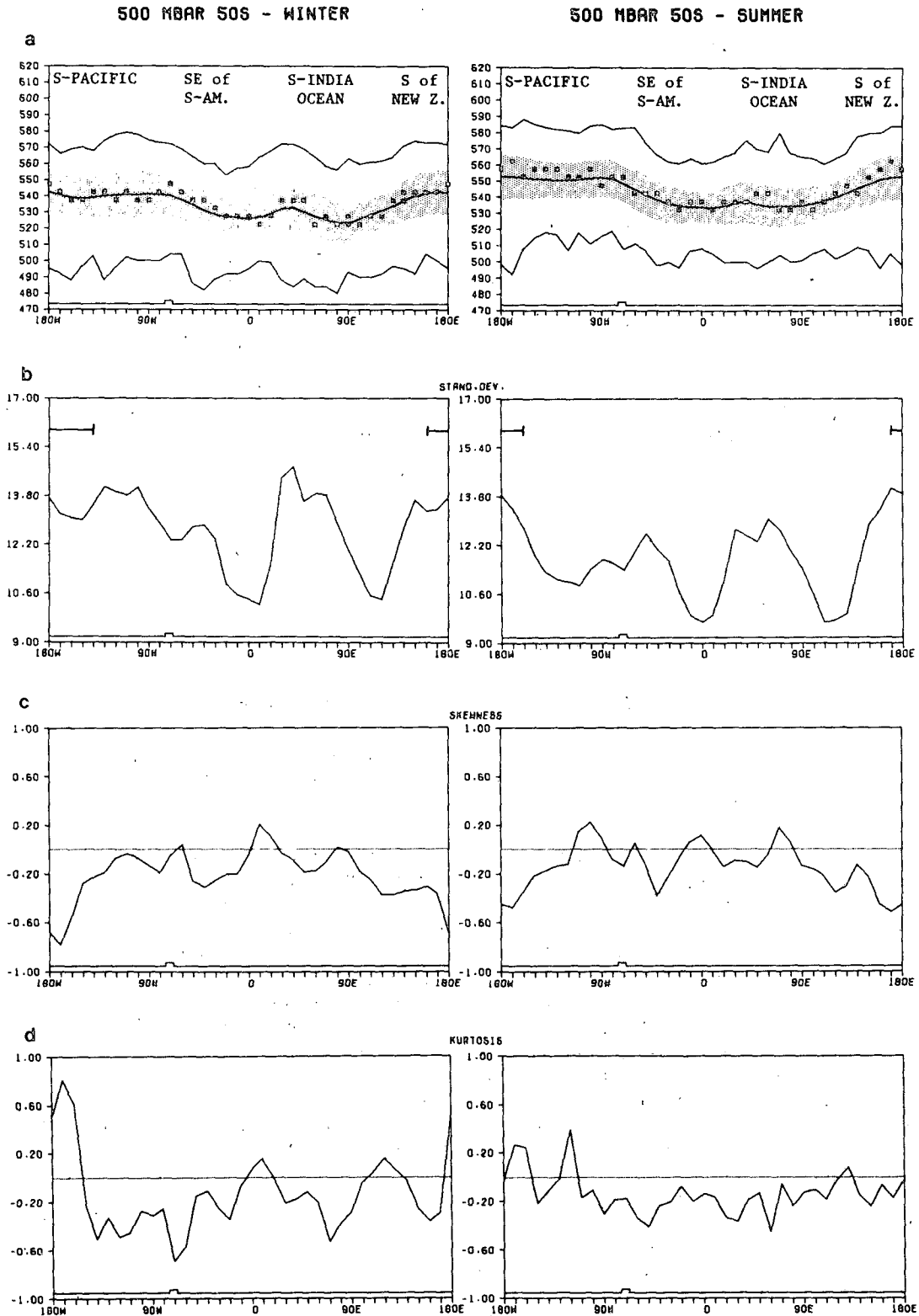
FIG. 4. Zonal variation of daily 500 mb geopotential height statistics along 50°S; from top to bottom: (a) seasonal averages (full line), modes (dots), standard deviations (shaded), positive and negative extrema (thin lines); (b) standard deviations and areas of significant deviation from Gaussian distribution (truncated straight line); (c) skewness; (d) excess or kurtosis.
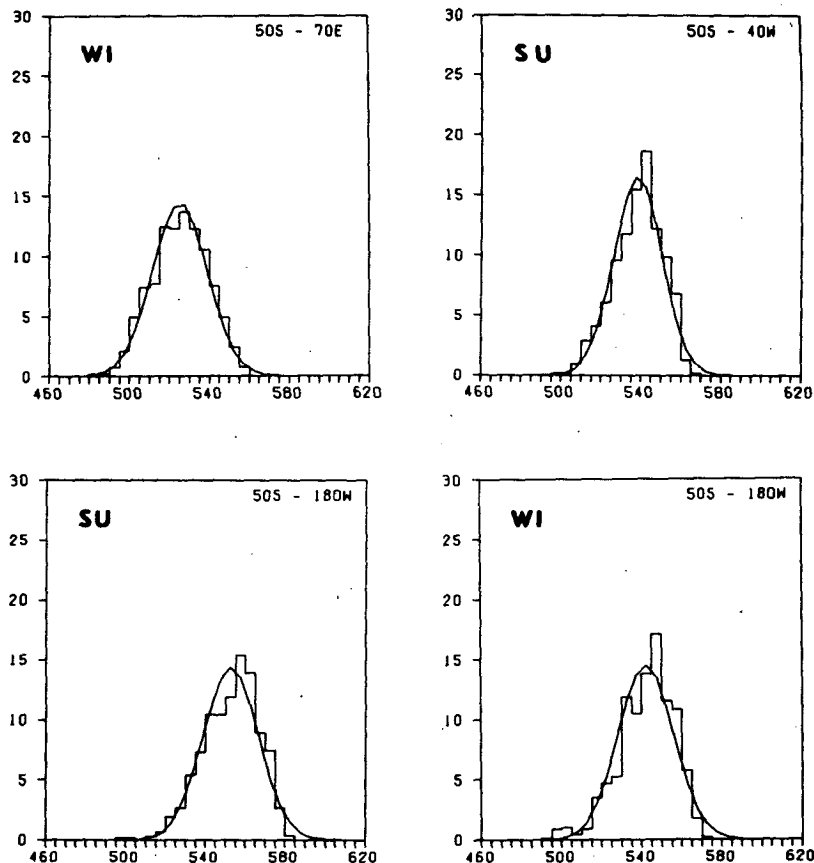
FIG. 5. Relative frequency distributions (%) of daily 500 mb geopotentials in the south Indian Ocean at 70°E, southeast of South America at 40°W and south of New Zealand at 180°W.

distribution as a whole (using a chi-squared test) and the higher moments (using a parameter test) deviate significantly from the Gaussian reference (indicated in Fig. 4b).

The zonal variations of the geopotential means (i.e., quasi-permanent troughs and ridges) $[Z(\lambda, t)]$, and standard deviations $(m_2^{1/2})$ seem to be in general agreement with other studies (van Loon, 1972; Trenberth, 1981a,b). Not unlike the NH midlatitudes, the regional statistics can be related to the position of the centers of action (White, 1980). In summer, three maxima of the standard deviation (Fig. 4b), indicating strong synoptic activity, occur in the areas south of New Zealand ($\sim$180°E), southeast of South America ($\sim$40°W) and in the south Indian Ocean ($\sim$70°E). In winter, the New Zealand maximum extends further eastward to the South Pacific (Fig. 4). But, only south of New Zealand the observed geopotential frequencies deviate significantly from Gaussian in both seasons; both the chi-squared and Kolmogoroff-Smirnov test have been applied at a 95% significance level.

Furthermore, two maxima of negative skewness are observed in the south of New Zealand and in the

southeast of South America, which coincide with the maximum variance areas (Fig. 4); i.e., the long (short) wing of the frequency distribution tends towards low (high) geopotentials. As this feature is associated with modal (most frequent) values above the mean, high pressure systems apparently have some predominance. Indeed, the region south of New Zealand is the main area in the SH where blocking anticyclones persistently form. They also occur, but only occasionally, in the southeast of South America (van Loon, 1956).

In comparison with the other maximum of negative skewness observed southeast of South America, the distribution in the area south of New Zealand reveals a relatively long tail towards frequent low extremas (Fig. 5); the observed track of cut-off cold lows crossing this region can produce this effect (Trenberth, 1981b). Both cut-off cold lows and blocking anticyclones lead to a geopotential-height distribution of large variance, which significantly deviates from Gaussian distribution and has large negative skewness in both seasons and high kurtosis in winter.

In case of producing local time spectra one should expect both short and long period weather distur-

bances in the areas south of New Zealand and southeast of South America. However, short period fluctuations should dominate the south Indian Ocean, where synoptic activity is observed to distribute its large variance almost Gaussian (Fig. 5), i.e., with low skewness and kurtosis.

6. Conclusion

Despite the limitations of the data set and, thus, of the various statistics, the results of this study emphasize differences and similarities between the midlatitude eddies of each hemisphere. The transient eddy variances along the 50°N and S latitude circle reveal two peaks of long and short eastward propagating waves in the wavenumber–frequency spectra. The third peak of ultra-long period fluctuations (of ~20 days), which is observed only in the NH circulation, reflects the different role of the quasi-stationary waves in both hemispheres: In the NH, heat is transported by ultra-long eastward propagating waves of baroclinic structure. But, westward propagating waves of the same period and wavenumber reveal a quasi-barotropic structure, thus giving no contribution to the meridional heat transport (Böttger and Fraedrich, 1980). In the SH, however, the ultra-long waves are reduced.

Zonal asymmetries are weaker in the SH, but there are still significant longitudinal differences in the regional frequency distributions of geopotential height. Maximum variance (and thus, synoptic activity) is observed over the southern Indian Ocean (in winter) and is almost Gaussian distributed. The other maxima in the south of New Zealand/South Pacific and the southeast of South America are of different synoptic origin, i.e., blocking anticyclones alternating with cyclonic storms and occasional cut-off cold lows lead to negatively skewed frequency distributions.

REFERENCES

Böttger, H., and K. Fraedrich, 1980: Disturbances in the wave-number–frequency domain observed along 50°N. *Contrib. Atmos. Phys.,* **53,** 90–105.
Fraedrich, K., and H. Böttger, 1978: A wavenumber–frequency analysis of the 500 mb geopotential at 50°N. *J. Atmos. Sci.,* **35,** 745–750.
Hayashi, Y., 1971: A generalized method of resolving disturbances into progressive and retrogressive waves by space Fourier and time cross-spectral analyses. *J. Meteor. Soc. Japan,* **49,** 125–128.
——, 1973: A method for analyzing transient waves by space–time cross spectra. *J. Appl. Meteor.,* **12,** 404–408.
——, 1977: On the coherence between progressive and retrogressive waves and a partition of space–time power spectra into standing and travelling parts. *J. Appl. Meteor.,* **16,** 365–373.
——, and D. G. Golder, 1977: Space–time spectral analysis of midlatitude disturbances appearing in a GFDL general circulation model. *J. Atmos. Sci.,* **34,** 237–262.
Loon, H. van, 1956: Blocking action in the Southern Hemisphere. *Notos,* **5,** 171–177.
——, 1965: A climatological study of the atmospheric circulation in the Southern Hemisphere during the IGY, Part 1. *J. Appl. Meteor.,* **4,** 479–491.
——, 1972: Pressure in the Southern Hemisphere. *Meteorology of the Southern Hemisphere, Meteor. Monogr.,* No. 35, Amer. Meteor. Soc., 59–86.
Notos, 1964–70: Historical Weather Charts for the Southern Hemisphere. Atmospheric Project Southern Hemisphere, *13–19,* South African Weather Bureau, Pretoria.
Taljaard, J. J., and H. van Loon, 1960: The construction of 500 mb contour maps over the Southern Ocean. *Antarctic Meteorology.* Pergamon Press, 96–114.
——, and ——, 1964: Southern Hemisphere weather maps for the International Geophysical Year. *Bull. Amer. Meteor. Soc.,* **45,** 88–95.
Trenberth, K. E., 1981a: Interannual variability of the Southern Hemisphere 500 mb flow: Regional characteristics. *Mon. Wea. Rev.,* **109,** 127–136.
——, 1981b: Observed Southern Hemisphere eddy statistics at 500 mb: Frequency and spatial dependence. *J. Atmos. Sci.,* **38,** 2585–2605.
White, G. H., 1980: Skewness, kurtosis and extreme values of Northern Hemisphere geopotential heights. *Mon. Wea. Rev.,* **108,** 1446–1455.